Refractive-index measurements of dense helium up to 16 GPa at $T=298$ K: Analysis of its thermodynamic and electronic properties

René Le Toullec, Paul Loubeyre, and Jean-Pierre Pinceaux
Laboratoire de Physique des Milieux Condensés, Université de Paris VI, 75230 Paris CEDEX 05, France
(Received 17 January 1989)

The refractive index of He as a function of pressure, $n(P)$, has been measured with an accuracy of 3×10^{-3}, in a diamond anvil cell up to 16 GPa at $T=298$ K, by an experimental procedure which couples two types of interferometric methods. These data permit us to obtain, from recent Brillouin scattering measurements, the fluid adiabatic sound velocity, so as to derive the equation of state of liquid He up to melting, the volume discontinuity at melting, and some related thermodynamic quantities. Under justified physical assumptions, the equation of state is extrapolated into the solid phase, in good agreement with recent single-crystal x-ray data. The comparison of these two equations of state with different calculations confirms the importance of many-body interactions in dense He. The refractive index of He, expressed as a function of density, is then related, through a Sellmeier formula, to the electronic properties of dense He: These are given in terms of the evolution with density of the excitonic $1^1S_0\rightarrow2^1P_1$ energy level and of the contraction of the electronic cloud of the He atom.

I. INTRODUCTION

With pressure, simple molecular solids which are insulators at low density, gradually become semiconductors and finally metallize. Such an evolution towards metallization is of fundamental interest: It requires working with the Coulombic Hamiltonian of the system, i.e., between the electrons and the nuclei, and various theoretical attempts for modeling that have been proposed, like tight-binding methods,[1] Hartree-Fock-type approaches,[2] and one-electron density-functional calculations.[3] But such calculations have yet to incorporate phenomenological inputs in order to obtain good agreement with experiment.[4,5] However, there is a very promising way for calculating such electronic properties quasiexactly through the use of quantum simulations.[6] The quantum simulation of a system of H_2 molecules has recently been performed over the whole density range from its insulating phase up to a monatomic metal.[7]

It then seems that theory is ahead of experiment since there is a shortage of experimental data on which to compare all those various calculations of the electronic properties of simple molecular systems, specially on He and H_2 which should be the best experimental references due to their electronic simplicity and also to their evolution going over a large density range, from insulating atomic or molecular solid to monatomic metal. It is consequently easily understandable why the measurements of the electronic properties of simple molecular systems at very high density is one of the major projects of high-pressure physics.

Such a lack of electronic property measurements stems from the fact that for generating high pressures on such systems (now routinely around 1 Mbar) diamond anvil cells have to be used. Although they are wonderful tools, their main drawback for the purpose discussed is that the diamond band edge is around 5 eV. This prevents the use of any direct absorption-type experiments which usually permit characterization of the system at low pressure as reviewed by Sonntag for rare gases.[8] Only at very high pressure, once the band edge of the transition drops below the one of diamond, are single-photon experiments possible; for example, absorption experiments have been reported for solid xenon only for pressures above 30 GPa.[9]

The only way to circumvent this problem is to measure physical properties which are directly related to the electronic transitions of the system and the refractive index seems to be the best candidate. Different methods for measuring the refractive index in a diamond anvil cell have already been proposed in the literature;[10,11] however their accuracy was inadequate so as to obtain unambiguously the electronic properties.

In Sec. II we present a new interferometic method which enables measurements of the refractive index for visible wavelengths in a diamond anvil cell with an accuracy of 3×10^{-3}. The method was here applied to the measurement of the refractive index of dense He.

Based on these $n(P)$ data and recent Brillouin scattering measurements, in Sec. III an analysis of the thermodynamic properties of dense He gives the equation of state (EOS) in the liquid and solid phases, the volume discontinuity at melting, and the adiabatic sound velocity as a function of density.

In Sec. IV the EOS is used to relate our refractive-index measurements of dense He to the evolution with density of its electronic properties in terms of the energy of the excitonic $1^1S_0\rightarrow2^1P_1$ level and of the contraction of the atomic electronic cloud in the crystal.

II. REFRACTIVE-INDEX MEASUREMENTS OF DENSE HELIUM

A. Membrane diamond anvil cell Fabry-Perot optical system

As sketched in Fig. 1, this setup is constituted of a diamond anvil cell for generating the pressure and of an optical setup assembled for measuring the refractive index by two interference techniques.

1. The diamond anvil cell

The main characteristics of diamond anvil cells have been extensively reviewed.[12,13] For an understanding of the present refractive-index measurement method, suffice it to say that the sample is enclosed in a cylinder formed by a hole drilled in a T 301 stainless-steel gasket which is compressed by the two culets of the diamond anvils; a small ruby ball is put in the sample chamber for the pressure measurements.[12] The two culets of the diamonds constitute a Fabry-Perot interferometer, with its intermediate medium filled with the sample under pressure: Plane-parallel plates interferometric methods can then be applied to measure the refractive index of this dielectric medium. For doing accurate measurements, the parallelism of the diamond culets has to be kept at best under pressure. That is why we have used a newly designed diamond anvil cell, the membrane diamond anvil cell (MDAC);[14] its main new feature is that the force on the piston is generated by pressurized helium which pushes an annular membrane. The thrust on the mobile piston is then axial and the variation of pressure very smooth; these are optimum conditions for keeping the parallelism of the culets under pressure. The detailed presentation of the cell and the method for loading the He sample have been described elsewhere.[14]

2. Interferometric measurements

The essence of a Fabry-Perot interferometric measurement is to coherently add two different beams of wave-

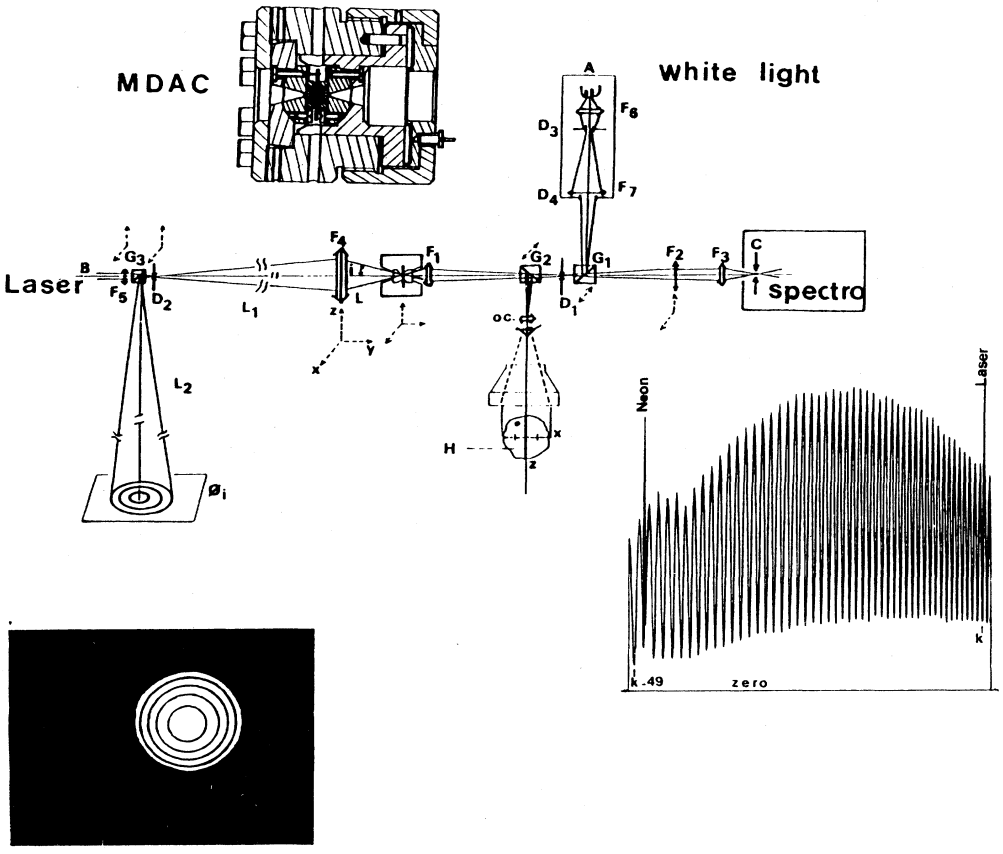

FIG. 1. Optical setup for interferometric measurements: (A) quartz-iodine lamp, (B) A^+ laser beam, (C) spectrometer slits, (G_i) separating cubes, (F_i) lenses (F_1 is a UM32 Wild-Leitz microscope objective and F_4 a 50 mm focal distance camera lens), (OC) $\times 20$ eyepiece; (L_1, L_2, L_3) distances of, respectively, 54, 675, 4250 mm, (H) image of the sample, Φ_i diameter of the diffraction ring, (MDAC) is a design of the MDAC. In the bottom right of the figure is shown the white-light interferences as recorded through the spectrometer; in the bottom left of the figure is shown a photograph of the rings of the laser interferences.

length λ of which optical paths differ by ne, n being the refractive index of the medium inside the Fabry-Perot and e its thickness. The fringe pattern is then directly related to ne/λ. Unfortunately, it is generally very difficult to extract n and e from such a measurement since they appear in the formula in the form of their product. We solved this problem by coupling two interferometric methods: the one corresponding to a white-light parallel beam and the other to a convergent monochromatic laser beam.

This was performed on the optical assembly, drawn in Fig. 1, which is set in front of the entrance slit of a spectrometer. Once the laser beam has been lined up with the spectrometer, diaphragms D_1 and D_2, separating cubes G_1, G_2, and G_3, and diaphragm D_4 are aligned in this order. The eyepiece is then positioned so that the laser beam goes through the center of its graduated reticle. Afterwards, lenses F_3,F_2,F_6,F_1,F_4,F_5 are placed on the bench. The lens F_3, the diaphragm D_1, the Wild-Leitz UM32 microscope objective F_1, the camera lens F_4, and the eyepiece have fixed positions; the separating cubes G_1 and G_2 are mounted on the two positions slides and the MDAC on an xyz micrometric stage. Our experimental procedure is decomposed in three steps.

Placing the cell. The sample chamber is visualized through the UM32 objective and the eyepiece which make a ($\times 380$) microscope. The cell is moved in the y direction until a good focus is obtained. The region of the sample, of which the refractive index and thickness will be measured, corresponds to the domain of 10 μm diameter around the center of the reticle.

White-light interference measurements. These interferences are obtained by illuminating the sample chamber under a parallel beam of white light of 25 μm diameter spot in the cell. It is produced by the quartz-iodine lamp A, two lenses F_6 and F_7, and two diaphragms 0.5 mm in diameter, D_3 and D_4. This setup is turned on by sliding cube G_1 into position. For incident light $I_0(\lambda)$, the reflected light going into the spectrometer $I_r(\lambda)$ is given by the well-known formula:

$$I_r(\lambda)=I_0(\lambda)\frac{F\sin^2(2\pi ne/\lambda)}{1+F\sin^2(2\pi ne/\lambda)} . \tag{1}$$

The fringe pattern measured out of the spectrometer is of a good contrast as shown on the right of Fig. 1. Around 60 interference fringes were recorded in a spectral domain taken between the wavelength $\lambda_l=5145.4$ Å of the laser beam and the one $\lambda_n=7425.2$ Å of a neon lamp. The order of interference of the laser wavelength K_l is then obtained by counting the number of minima of interference Δk between the wavelength λ_1 of the minima of interference nearest to λ_l and the one λ_2 nearest to λ_n, i.e.,

$$K_l=\Delta k\,\lambda_2/(\lambda_2-\lambda_1) . \tag{2}$$

This formula is in fact really exact if there is no dispersion. In He the dispersion is quite small and K_l calculated by the above formula was differing from its true integer value by a positive quantity less than 0.4 up to 16 GPa. This was consistently checked with the Sellmeier equation used below to analyze the refractive index data.

Laser interference measurements. The laser beam is diverged by F_5 to fill the camera lens F_4 which enables a 4 μm diameter focus in the sample chamber; cube G_3 and the iris D_2 separate off the coherent beam reflected on the two diamond culets. Projected on a screen, this gives a contrasted fringe pattern very similar to the one given by plane parallel plates, as seen in the bottom left of Fig. 1. This fringe pattern can, however, be obtained in any plane situated behind F_4.

The dark interference rings of diameter Φ_i, measured on the screen, are given by the following relations:

$$2e(n^2-\sin^2 i)^{1/2}=K_i\lambda_l , \tag{3a}$$

$$\phi_i=A\tan i . \tag{3b}$$

A is a geometrical factor which relates Φ_i to the angle i of its corresponding beam after F_4. A is experimentally calibrated by measuring the refractive index of air. The order of interference K_i of the ith ring is straightforwardly related to K_l by $K_i=K_l-i$. From Eq. (3) it is easily obtained that

$$n^2=\left[\frac{\phi_2^2K_1^2}{A^2+\phi_2^2}-\frac{\phi_1^2K_2^2}{A^2+\phi_1^2}\right](K_1^2-K_2^2)^{-1} \tag{4}$$

which enables a direct determination of the refractive index n of the sample from the measurement of the diameter of two rings; its thickness e is then obtained from Eq. (3).

Before we move to the analysis of the data obtained on He, three comments have to be made in order to stress the care which had to be taken from reaching an accuracy as high as 3×10^{-3}.

(i) In principle, the refractive index could be obtained from Eq. (4) with two diffraction rings only. In fact, we had to use all the different couples associated to four rings at least. With a program, the diameters of the rings were slightly changed within experimental error bars ($\Delta\Phi/\Phi=3\times10^{-3}$) so as to obtain the smallest dispersion of the values of n calculated with the different pairs of rings. It is easily shown that the number of fringes ΔK is related to the thickness e of the sample through

$$\Delta K=\frac{e\sin^2 i_m}{\lambda n_l} , \tag{5}$$

where i_m is the maximum optical aperture angle of the MDAC ($i_m=15°$); a Δk equal to 4 necessitates a thickness of 50 μm at 16 GPa which could only be obtained by using a double gasket.

(ii) Theoretically, the geometrical factor A is given by

$$A=L_2(L-F)/F , \tag{6}$$

where F is the focal distance of the camera lens F_4 and L is the image distance of the diamond culet c_1 the nearest to F_4. $L-F$ being of the order of 4 mm, c_1 had to be positioned with an accuracy better than 4 μm so to be always in the same geometrical configuration.

(iii) The variation of n caused by nonhydrostaticity and

the variation of thickness e due to the nonparallelism of the culets or to their deformation, could be sensitively detected on the changes of the ring fringe pattern when the sample chamber was moved in the x or z directions. That explains why it was very important to be sure that both interferometric measurements were done in the same region of the sample.

B. Results

The measurements of the refractive index of He in the liquid and the solid phases up to 16 GPa at $T=298$ K are plotted in Fig. 2. The dispersion of the experimental points gives the magnitude of the uncertainty in the absolute determination of the refractive index, i.e., 3×10^{-3}. However, the fit of these measurements, represented by the solid line in Fig. 2, somehow averages out these errors and should give $n(P)$ with an accuracy of 1×10^{-3}.

The minimum pressure attainable with the MDAC is 0.2 GPa, below which He fluid leaks out of the sample chamber. The measurements are reported only up to 16 GPa since above the accuracy of the measurements worsens with pressure: for a given accuracy the thickness of the sample, e should increase with n [see Eq. (5)] and so should be greater than 50 μm above 16 GPa, a requirement that we could not fulfill even with double gaskets. Upon to 1 GPa, the refractive-index measurements (in the static region) of Lallemand and Vidal,[15] agree within the 3×10^{-3} error bars with the present results (measured at $\lambda=5145.4$ Å but converted into static values with the Sellmeir formula [Eq. (19)] which is used below to analyze the data); however, it should be noted that they increasingly differ with pressure from our $n(P)$ fit, being systematically lower. Finally, the discontinuity of n at melting was measured, giving $\Delta n/n=0.33\%$ ($n_l=1.1772$ and $n_s=1.1811$); this will be related in Sec. III B to the volume discontinuity at melting.

Some data are given in Table I, since we believe that they should be useful for high-pressure research: He is known as the best hydrostatic medium and should thus really be utilized in the studies of solids under high pressure in order to minimize the parasitic influence of strains on the EOS and on the phase diagram; the characterization of a semiconductor under pressure is mainly based on optical studies, the analysis of which will sometimes require the refractive-index values of the pressure-transmitting medium.

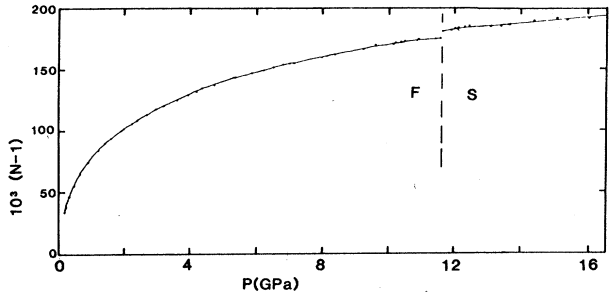

FIG. 2. Refractive index of He as a function of pressure at $T=298$ K. The dots are the experimental points, and the solid line their fit; the vertical dash line marks the melting pressure ($P=11.6$ GPa).

As it will be shown below, the electronic properties of dense He can only be obtained from the refractive index if we know its density dependence. Consequently, in the next section we will first reanalyze recent Brillouin scattering measurements of Polian and Grimsditch[16] in order to obtain an equation of state of liquid He up to its melting density. The one previously derived by them from their Brillouin measurements could be subject to criticisms since they had to use an extrapolation of $n(P)$ and their hypotheses on C_p/C_v were questionable. From it, a complete set of thermodynamic properties of dense He will be calculated under some reasonable physical assumptions.

TABLE I. Physical properties of dense He at $T=298$ K; melting is occurring at $P=11.6$ GPa. V is the volume [from V_+ of Eq. (10)], P the pressure, n the refractive index, U the adiabatic sound velocity, γ the ratio of specific heats [from $1/\gamma_+$ of Eq. (9)], E_0 the excitonic $1^1S_0\rightarrow2^1P_1$ energy level, C the Clausius-Mossotti factor.

V (cm^3/mol)	P (GPa)	$10^3(n-1)$	U (km/s)	$\gamma=C_p/C_v$	E_0 (eV)	C (cm^3/mol)
22.512	0.2	35.0	1.673	1.510	21.58	0.5170
13.760	0.5	57.5	2.258	1.404	21.59	0.5166
10.175	1.0	78.0	2.879	1.310	21.61	0.5164
7.833	2.0	101.0	3.666	1.224	21.63	0.5156
6.177	4.0	129.0	4.638	1.153	21.70	0.5134
5.411	6.0	147.2	5.289	1.112	21.79	0.5113
4.935	8.0	160.7	5.796	1.084	21.94	0.5076
4.597	10.0	170.8	6.218	1.064	22.17	0.5015
4.387	11.6	177.2	6.497	1.052	22.40	0.4958
4.262	11.6	181.1			22.57	0.4919
4.107	13.0	186.0			22.80	0.4864
3.965	14.5	190.0			23.12	0.4792
3.840	16.0	193.0			23.48	0.4713

III. THERMODYNAMIC PROPERTIES OF DENSE He AT $T=298$ K

A. Liquid phase

In a recent article, Polian and Grimsditch[16] have reported Brillouin frequency shifts in fluid He as a function of pressure up to melting. Their Brillouin scattering measurements were done in the backscattering geometry and so in order to obtain the adiabatic sound velocity U from the measured frequency shift $\Delta\omega=2n\omega_l U/c$, the refractive index as a function of pressure $n(P)$ has to be known. The equation of state can then be related to U through the following thermodynamic equation:

$$B_T=\frac{\rho U^2}{\gamma} , \tag{7}$$

where γ is the ratio of the specific heats ($\gamma=C_p/C_v$), ρ the density, and B_T is the isothermal bulk modulus.

The present $n(P)$ data are therefore used to derive from these Brillouin measurements[16] the precise experimental $U(P)$ from 1 GPa up to 12 GPa; they are completed by the experimental values of McCarthy[17] below 0.2 GPa, of Kortbeek *et al.*[18] up to 1 GPa, and those of Mills *et al.*[19] up to 2 GPa. Rewriting Eq. (7) as

$$\int_{P_0}^{P} dP' \frac{1}{U^2(P')}=\int_{\rho_0}^{\rho} d\rho \frac{1}{\gamma(\rho)} \tag{8}$$

gives the numerical procedure for obtaining the fluid equation of state from sound-velocity data if $\gamma(\rho)$ is known. Unfortunately, $\gamma(\rho)$ has only been measured up to 1 GPa ($\rho=0.4$ g/cm^3). In Fig. 3 the experimental determinations of $\gamma(\rho)$ of various authors[17,18,20] are compared. They were though not directly measured but obtained from Eq. (7) by combining compressibility and sound-velocity measurements; such a procedure relies heavily on the numerical fits of the data and that explains why there is such a scattering in the experimental points. In their recent work, Kortbeek *et al.* have considered those sources of error and so their values of $\gamma(\rho)$ are expected to be quite accurate. For extrapolation $\gamma(\rho)$ up to melting, we use two calculations: the one of Ross[21] based on its liquid variational theory[22] with the exponential-six potential[23] and our one in the solid phase, based on the self-consistent phonon with cubic anharmonic term calculation[24] with the exponential-six[23] or Aziz[25] pair potentials. The quite large differences between these two calculations can be imputed either to the discontinuity of γ at melting or to the errors inherent in the calculations which have to be very accurate since γ is related to the second derivative of the free energy with respect to T. We then set two extrapolations: one which is based on the calculation of Ross $1/\gamma_-$ and the other one agreeing with Kortbeek's data and our calculation $1/\gamma_+$. These two functions were fitted by polynomials, giving

$$1/\gamma_-=0.6+0.358\rho+0.127\rho^2-0.18\rho^3 , \tag{9a}$$

$$1/\gamma_+=0.6+0.27\rho+0.615\rho^2-0.721\rho^3+0.206\rho^4 , \tag{9b}$$

where ρ is in g/cm^3.

From these two $\gamma(\rho)$ curves, two equations of state were derived from Eq. (8), V_- is associated and $1/\gamma_-$ and V_+ to $1/\gamma_+$. We have applied successfully the following empirical equation, introduced by Benedict,[19] to fit them:

$$\begin{aligned} V_+(\text{cm}^3/\text{mol})&=23.810P^{-1/3}-17.833P^{-2/3} \\ &\quad +29.760P^{-1} , \\ V_-(\text{cm}^3/\text{mol})&=23.256P^{-1/3}-16.36P^{-2/3} \\ &\quad +29.226P^{-1} , \end{aligned} \tag{10}$$

where P is in kbar.

The self-consistency of our numerical procedure was checked by recalculating $\gamma(\rho)$ from our fits of $V(P)$ and $U(\rho)$ with Eq. (7). The agreement was excellent with a maximum deviation of 0.5% over the loop. The difference between our two determinations of the fluid EOS increases with density and amounts of 2% at melting. However, since the overall agreement of $1/\gamma_+$ with the experimental points is better than the one of $1/\gamma_-$, we believe that its corresponding EOS, V_+, should be nearer to the real one than V_-. Furthermore we will see below, when we will extrapolate the liquid equation of state in the solid phase under justified physical hypotheses, that the one obtained from V_+ is very near to the recent single-crystal x-ray diffraction measurements of Mao *et al.*[26]. This consequently tends to demonstrate that $1/\gamma_+$ and V_+ should be in fact very good fits of their corresponding true experimental values. So in all the following, the equation of state $V(P)$ and the ratio of the specific heats $\gamma(\rho)$ of liquid He will be, respectively, related to their fits $V_+(\rho)$ and $1/\gamma_+(\rho)$.

In Fig. 4 various experimental and theoretical EOS of

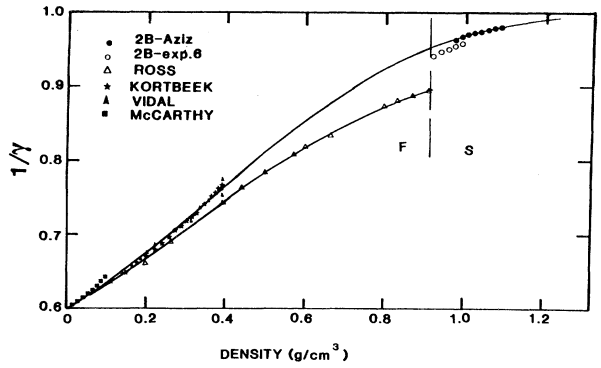

FIG. 3. The ratio of the specific heats $\Gamma=C_p/C_v$ as a function of density. The solid squares, solid triangles, and stars are, respectively, the experimental results of McCarthy (Ref. 17), Vidal (Ref. 20), and Kortbeek (Ref. 18). The open triangles, open circles, and solid circles are, respectively, the calculations of Ross (Ref. 21) in the liquid phase with the exponential-six potential, our calculations in the solid phase with the exponential-six and Aziz pair potentials. The solid lines represent $1/\gamma_+$ and $1/\gamma_-$ given by Eq. (9).

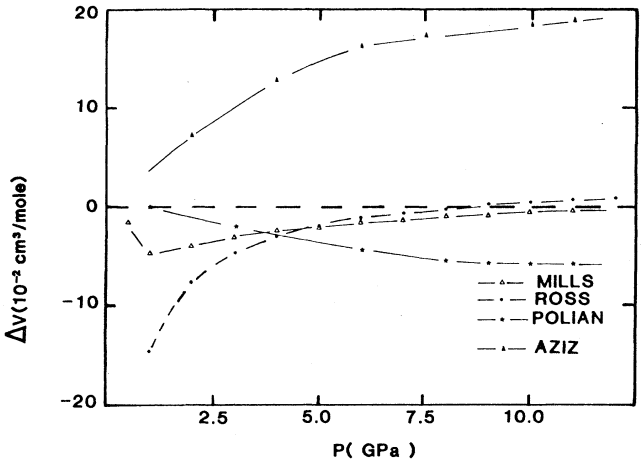

FIG. 4. Deviation of various liquid-He EOS at $T=298$ K from our determination [$V+$ of Eq. (10)]: the dash-open-triangle and dash-star lines are, respectively, the experimental fits of Mills (Ref. 19) and Polian (Ref. 16). The dash-dot and dash-solid-triangle lines are, respectively, the calculation of Ross (Ref. 21) with the exponential-six potential and the one of Barrat (Ref. 27) with the Aziz pair potential.

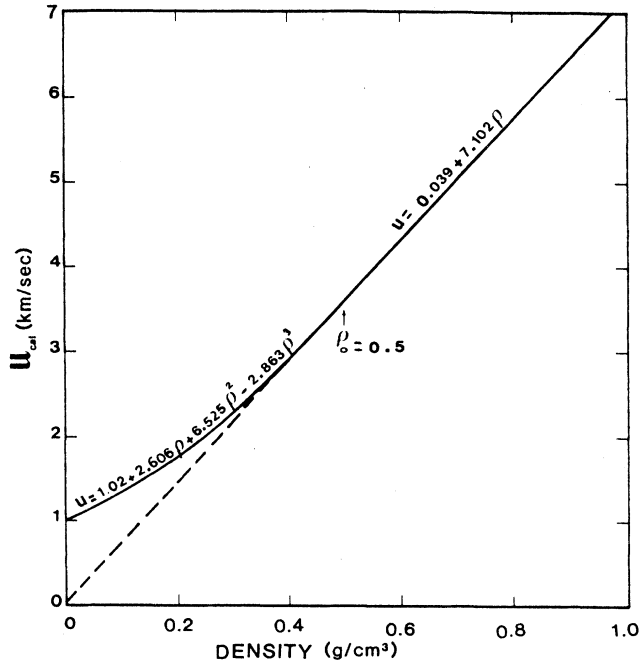

FIG. 5. Adiabatic sound velocity of He, U vs density at $T=298$ K. Below $\rho_0=0.5$ g/cm^3, the experimental data are very well reproduced (with an accuracy of 10^{-3}) by $U=1.02+2.606\rho+6.525\rho^2-2.863\rho^3$ and above by $U=0.039+7.102\rho$.

fluid He are compared to the present determination. The one of Polian,[16] based on the same Brillouin scattering measurements, increasingly differs with density, leading to a difference of 1.3% near melting; this discrepancy can be mainly imputed to their poor extrapolation of $\gamma(\rho)$. The extrapolation of the measurements of Mills,[19] made below 2 GPa, and fitted by a Benedict-type EOS, is in very good agreement (better than 2×10^{-3}). This comes from the fact that the Benedict-type EOS [of the form of Eq. (10)] seems to represent very well dense fluid over a large-density domain. Two calculations are also reported: the one of Ross[21] based on his variational method (including the $\hbar^2$ quantum correction) with the exponential-six potential and a quantum Monte Carlo path integral one[27] with the Aziz pair potential.[25] These two methods are known to give quasiexact EOS for a given interaction and so any observed difference from experiment should be attributed to the pair potential. When using the exponential-six potential the agreement is very good at least above 2.5 GPa, but there is an increasing discrepancy with density when the Aziz pair potential is chosen instead. This confirms recent conclusions on the importance of many-body interaction in dense He:[28,29] The Aziz pair potential has been adjusted on true pair properties, whereas the Ross potential has been derived from shock-wave Hugoniot, and so it incorporates averaged many-body interactions. At low density, the exponential-six potential certainly overestimates the contributions of many-body forces which are small, as it can be inferred from the good agreement obtained in this region when the Aziz pair potential is used.

In Fig. 5 we have plotted the adiabatic sound velocity U as a function of density over the whole density range of the liquid phase. Its main feature is that the adiabatic sound velocity is a linear function of ρ above $\rho_0=0.50$ g/cm^3. It clearly demonstrates that the well-known Rao's rule, expressed by $VU^{1/3}=$const, as well as the free-volume model, expressed by $V^{1/3}U=$const, are inappropriate for dense liquids. This linearity of the adiabatic sound velocity function of the density, known as the Birch law,[30] seems also to be valid in dense simple molecular systems even up to at least 1 Mbar, and this "universal" behavior will be analyzed more thoroughly in another article.[31] The linear behavior at very low density is related to the virial expansion.[32]

Some liquid thermodynamic properties are collected in Table I.

B. Volume discontinuity at melting

At the present time, the measurements of melting at very high density have been limited to the locus of the $P(T)$ melting line;[33] but, the volume discontinuity is needed for a complete description of the thermodynamic of the transition. Consequently, it seems interesting to relate the observed discontinuity of the refractive index at melting to its volume discontinuity. As it will be discussed below, the refractive index is related to the density by the well-known Lorenz-Lorentz relation:

$$\frac{n^2-1}{n^2+2}=\rho F_{11}(\rho)\ . \tag{11}$$

It is then straightforward to see that

$$\frac{6n^2}{(n^2+2)(n^2-1)}\frac{\Delta n}{n}=\left[1+\left[\frac{dF_{11}}{d\rho}\right]\frac{\rho}{F_{11}}\right]\frac{\Delta\rho}{\rho}\ . \qquad (12)$$

The $F_{11}(\rho)$ function is achieved below and, in the frame of the analysis of Sec. IV, is obtained to be independent of the phase, as seen on Fig. 8. From Eq. (12) and the measured $\Delta n/n$ equal to 0.33%, we obtained $\Delta\rho/\rho=2.8\%$ at $T=298$ K, corresponding to a melting pressure of 11.6 GPa, in very good agreement with the extrapolations of Mills *et al.*[19] or van der Putten *et al.*[34] and the calculation of Young *et al.*[23] as analyzed in Ref. 33. The volume discontinuity amounts to $\Delta V=0.125$ cm^3/mol. This is the first time that such a volume discontinuity at melting is measured in a diamond anvil cell, and this should motivate further studies since this quantity is a very sensitive test of the calculations of melting.[33]

C. Solid equation of state

The method which we used above to derive the equation of state of dense liquid He cannot be pursued in the solid phase, although Brillouin scattering measurements have been reported up to 20 GPa;[16] the solid bulk modulus is not easily related to the experimental data because of the anisotropy of the solid state.

Another method would be to extrapolate the function $F_{11}(\rho)$, which appears below in the analysis of the refractive index measurements, and then derive the EOS from $n(P)$. However, the equation of state obtained in doing so was found to be sensitively dependent on the numerical form assumed for the extrapolation.

We thus turn to a third method which is based on the following physical assumption: at high density, the equation of state of the liquid and the solid phases, extrapolated in their metastable region, are parallel and shifted by a constant quantity, the volume discontinuity at melting. Such a statement was clearly demonstrated by recent simulations of dense He around its room temperature melting.[35] The equation of state of solid He is then straightforwardly derived from the liquid equation of state, knowing the volume discontinuity at melting, $\Delta V=0.125$ cm^3/mol:

$$V(\text{cm}^3/\text{mol})=23.810P^{-1/3}-17.883p^{-2/3}+29.760P^{-1}-0.125\ , \qquad (13)$$

where P is in kbar. The difference with the true experimental EOS should be attributed mainly to the uncertainties in the determination of the liquid EOS which were analyzed above.

In Fig. 6 this EOS is compared to various calculations and to the recent single-crystal x-ray measurements.[26] We note a slight discrepancy with the x-ray measurements. Knowing that in the x-ray experiments the pressure was measured by the ruby fluorescence R_1 line excited by the synchrotron beam, it is possible that a small-temperature heating could have occurred with the consequence of introducing a systematic error in the pressure measurement; the observed difference of 5 Kbar would then correspond to an elevation of temperature in the ruby chip of the order of 40 °C which is a reasonable physical value. In any case, this discrepancy between the present and the x-ray EOS gives in fact the error bars which should be put on our experimental EOS, i.e., at most 1% on the volume. As already noticed above, this in return proves that our $V_+(P)$ liquid EOS should differ by less than 1% from the true experimental one. We have also performed calculations of the solid-He EOS with our self-consistent phonon model, using two pair potentials: the Aziz pair potential[25] and the exponential-six one.[23] Their comparison to the experimental one [Eq. (13)] in Fig. 6 confirms the trend already observed in the liquid phase: the EOS corresponding to the Aziz pair potential diverges with density from the experimental one while the agreement is quite good for the exponential-six potential, at least up to 20 GPa where it starts to diverge. As analyzed elsewhere, this is a direct proof of the importance of many-body interactions in dense He. Le Sar,[29] on one side, has recently proposed that these are due to the contraction of the atomic wave functions, induced by the high-pressure crystal environment; his pressure-volume curve is reported in Fig. 6. On the other side, Loubeyre[28] has shown that they can be well taken into account by an effective three-body exchange potential; the EOS calculated by adding this interaction to the Aziz pair potential is also reported in Fig. 6. It is interesting to note that the experimental EOS falls between these two theoretical predictions. It is not the purpose of the present article to critically discuss the two models of many-body interactions but much more to stress that further x-ray measurements are needed in order to reduce the experimental uncertainty on the EOS of solid He which is a necessary step towards the quasiexact descrip-

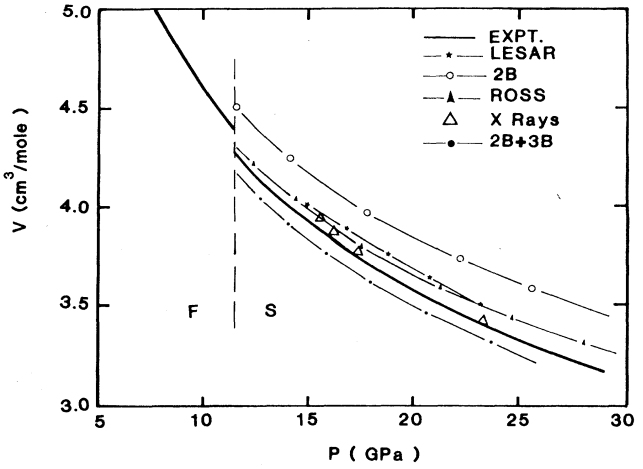

FIG. 6. Volume of solid He as a function of pressure at $T=298$ K. The solid line gives our determination [Eq. (13)]; the open triangles are single-crystal x-ray diffraction measurements (Ref. 26); the dash-star line is the theoretical EOS of LeSar (Ref. 29); the dash-solid-triangle, the dash-open-circle, and dash-solid-circle lines are our self-consistent phonon calculations with, respectively, the exponential-six potential (Ref. 25), the Aziz pair potential (Ref. 25), and the Aziz pair potential completed by three-body interactions (Ref. 28).

tion of dense He, as a model of dense insulators.

Should we stop here the analysis of our $n(P)$ measurements, we would miss one of the main information enclosed in them, that is the evolution of the electronic properties of He with density. The next part is devoted to such a study.

IV. ELECTRONIC PROPERTIES OF DENSE He

According to the theory of dielectric materials based on the Lorentz local-field model, the refractive index is related to the atomic polarizability through the Lorentz-Lorenz relation:

$$\frac{1}{\rho}\frac{n^2-1}{n^2+2}=\frac{4\pi N_a\alpha}{3}=F_{11}\ . \tag{14}$$

F_{11} is called the Lorenz-Lorentz factor expressed in the same units as the inverse of the density ρ, N_a is the Avogadro's number, and α represents a mean individual atomic polarizability which depends on the collective influence of the dense surrounding medium. It should be noted that this relation is exactly valid only for point dipoles in a cubic arrangement, otherwise the following occurs.

(i) In the liquid phase, deviations from this formula come from the different configurations of the molecules relative to one another which give statistical fluctuations on the induced dipole moments. According to Alder *et al.*,[36] the left-hand side of Eq. (14) should be rewritten as

$$F_{11}=\frac{4\pi N_a}{3}\alpha\left[1+\frac{5\alpha^2}{2\sigma^6}R^{zz}(0)\right], \tag{15}$$

where σ is the Lenard-Jones diameter. Because the dipole dielectric function $R^{zz}(0)$ is only important near the critical density and α^2/σ^6 is very small for He, this effect is certainly negligible[36] for the analysis of the present measurements at $T=300$ K.

(ii) Taking into account the spatial extent of the atomic charge distribution, the effective field on the atom should be written

$$\mathbf{E}_{\text{eff}}=\mathbf{E}+4\pi g\mathbf{P}/3 \tag{16}$$

where $\mathbf{P}$ is the vector of polarization of the medium and g is a measure of the charge overlap between neighbor atoms; for $g=1$, $\mathbf{E}_{\text{eff}}$ is the Lorentz local field which leads to Eq. (14). Guertin and Stern have calculated the value of g for Gaussian charge distributions in various lattices.[37] They have related g to the fraction f of the electronic charge contained in the atomic polyhedron. If we suppose that the spatial extent of the charge distribution of an He atom is given by its hard-sphere diameter σ ($=2.556$ Å), a rough estimate of f is then $f=6V/\pi\sigma^3$. From the values of Guertin and Stern,[37] we obtain that $0.98<g<1$ over all our experimental density range, g being even greater than 0.995 in the whole liquid phase.

This discussion demonstrates that we should obtain meaningful values of the atomic polarizability α in dense He, if we analyze our data with Eq. (14).

The atomic polarizability α is entirely related to the electronic transitions and Eq. (14) may be expressed in a quantum-mechanical Sellmeier form[38]

$$\frac{1}{\rho}\frac{n^2-1}{n^2+2}=\frac{4\pi\hbar^2N_ae^2}{3m_e}\times\left[\sum_{l,k}\frac{F_{lk}}{E_{lk}^2-E^2}+\int_{E_i}^{\infty}\frac{dF/dE'}{(E')^2-E^2}dE'\right], \tag{17}$$

where F_{lk} are the oscillator strengths associated with the discrete atomic transitions, and (dF/dE') are the photoionization cross sections for transitions to the continuum. The dielectric properties of He in the density range studied here, result mainly from the lowest uv levels which correspond to perturbations with density of the singly excited atomic transitions of the form $1^1S\rightarrow n^1P$. The dominant contribution is still the one associated with the $1^1S\rightarrow 2^1P$ transition since its oscillator strength is greater than the sum of the ones of all the other levels. Their total contribution could then be represented to a very good approximation by a single density-dependent Frenkel exciton line, denominated somehow improperly $1^1S_0\rightarrow 2^1P_1$. Equation (17) can then be reexpressed in the simpler form:

$$\frac{1}{\rho}\frac{n^2-1}{n^2+2}=\frac{4\pi\hbar^2N_ae^2}{3m_e}\left[\frac{f_0}{E_0^2(\rho)-E^2}+\frac{f_c}{E_c^2-E^2}\right], \tag{18}$$

where $E_0(\rho)$ and f_0 are, respectively, the density-dependent energy and oscillator strength (supposed to be independent of density as in the first-order perturbation) of the effective excitonic level. The remaining electronic transitions, i.e., the doubly excited and the ground-state continuum ones, have been lumped into the second term, corresponding to an effective transition of oscillator strength f_c and energy E_c, supposed to be independent of the density. This dispersion formula serves several purposes: It expresses data economically, permits interpolation, averages over random errors, and has theoretical implications.

Its parameters are directly obtained from Eq. (43) of Peck,[39] which was fitted on dispersion data of the refractive index of He gas at $T=0$ °C and $P=1$ atm. The numerically explicit form of Eq. (18) is then

$$F_{11}=276.87\left[\frac{0.496}{E_0^2(\rho)-E^2}+\frac{1.212}{(38.86)^2-E^2}\right]. \tag{19}$$

in which the energy of the electromagnetic wave is in eV and ρ is in mole/cm^3. In the dilute gas, $E_0=21.57$ eV whereas the atomic $1^1S\rightarrow 2^1P$ atomic energy level is equal to $E=21.22$ eV. This demonstrates the fact that although this excitonic level takes effectively into account many other singly excited transitions, its energy differs little from the one of the $1^1S\rightarrow 2^1P$ atomic level or of its perturbation with density. This formula was then applied to analyze the measurements of the absolute reflectance R of liquid He at 1.2 K performed by Surko *et al.*[40]

$$R=\frac{(n-1)^2+K^2}{(n+1)^2+K^2} \tag{20}$$

in which an absorption K is due to the damping factor Γ which is included in Eq. (19) by replacing the first term of the right-hand side Eq. (19) by

$$0.496/(E_0^2-E^2-i\Gamma E)\ . \tag{21}$$

As seen in Fig. 7, a very good agreement was obtained with $E_0=21.59$ eV and $\Gamma=0.432$ eV; at such a low density ($\rho=0.1449$ g/cm^3, a value which was extrapolated from the measurements of Edwards[41]), a shift of this excitonic level E_0 is already measurable. We have also pointed in Fig. 7, the calculated position $E_g=21.48$ eV of the maximum of the absorption peak, which is related to $2nK$. Equation (19) was also applied to analyze the refractive-index measurements of Edwards[41] at $\rho=0.13307$ g/cm^3, giving $E_0=21.58$ eV. These two very accurate values of E_0 at low density and the analysis of our refractive-index measurements with the experimental EOS derived in the preceding section, give the evolution of the energy of the effective excitonic $1^1S_0\rightarrow 2^1P_1$ line, $E_0(\rho)$, over a large density range, as plotted in Fig. 8. Furthermore, we can say that its relative variation should be very near to the one of the true $1^1S_0\rightarrow 2^1P_1$ excitonic level. Nevertheless, extrapolating $E_0(\rho)$ would give an unphysical always increasing $E_0(\rho)$. It is because in our model [Eq. (18)], we have neglected the variation with density of the oscillator strength, f_0. This hypothesis certainly breaks down at high density, but in the domain of validity of the first-order perturbation theory, roughly corresponding to the density range investigated here, it should be correct. Some numerical values of $E_0(\rho)$ are given in Table I.

This blue shift of the exciton energy has previously been observed by Sinnock and Smith in their study of the refractive index of condensed argon, krypton, and xenon at atmospheric pressure.[42] This is qualitatively understandable since as the density is increased, the exciton energy increases due to the increased interactions of the more diffuse excited state with the rest of the crystal.

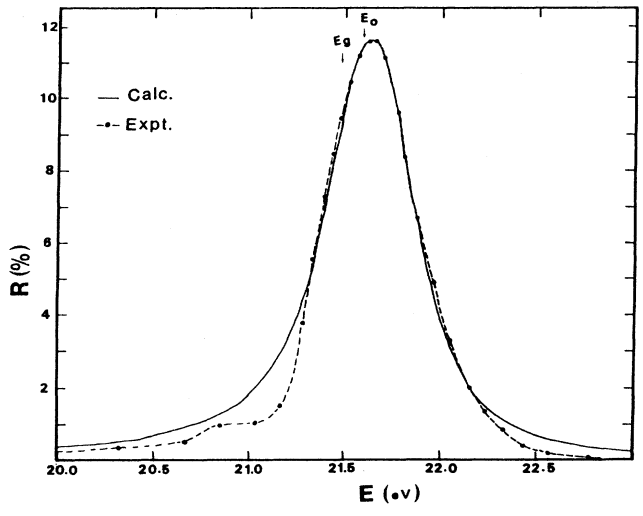

FIG. 7. Absolute reflectance of liquid He at 1.2 K. The dots are the measurements of Surko (Ref. 20); the solid line our calculation [Eq. (21)] with a damping factor $\Gamma=0.432$ eV and an excitonic level $E_0=21.59$ eV.

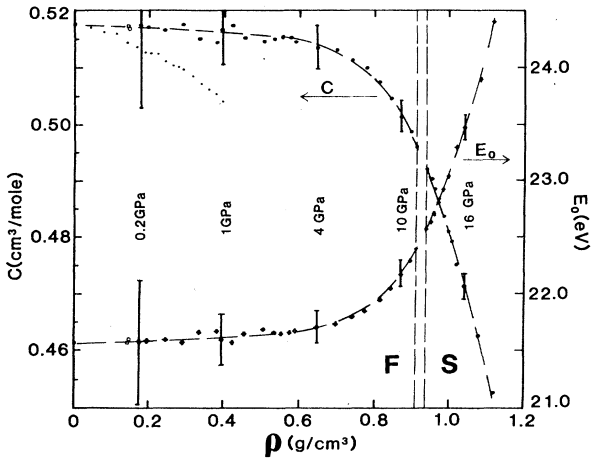

FIG. 8. Evolution of the Clausius-Mossotti factor C and of the energy of the $1^1S_0\rightarrow 2^2P_1$ excitonic level E_0 with density. The small dots are the experimental results of Lallemand (Ref. 15) the open circles and open squares are data obtained, respectively, from the measurements of Surko (Ref. 40) and Edwards (Ref. 41). The dots (C) and crosses (E_0) are obtained from the present $n(P)$ measurements; the dash lines interpolate between them as guide to the eyes.

Although the electronic transitions in the He atom are in the far uv region, there is still a frequency dependence of the refractive index in the visible. Equation (19) was then used to extrapolate our data in the static limit in order to make a comparison with previous dielectric measurements. A systematic study of the dielectric properties of rare-gas crystals under pressure up to 1 GPa has been performed by Lallemand and Vidal with capacitance measurements.[15] In the static limit, Eq. (14) is usually called the Clausius-Mossotti relation and its right-hand side the Clausius-Mossotti factor C. The values of $C(\rho)$ obtained from the present measurements as well as from the ones of Surko[40] and Edwards[41] are reported in Fig. 8. The error bars correspond to an error of $\pm 10^{-3}$ around the $n(P)$ values given by the fit of the present measurements. The error bars are very large at low density but fortunately they decrease with density as seen in Fig. 8. The differences between our $C(\rho)$ and the one of Lallemand[15] are within these large low-density error bars. However, if we take into account the very accurate measurements of Surko[40] and Edwards,[41] which are in very good agreement, and the behavior of our $C(\rho)$ at high density, where the error bars are small, we then see that the evolution proposed by Lallemand is certainly too steep. We feel confident that the dashed line, representing the $C(\rho)$ results in Fig. 8, reflects very well the evolution of the He atomic polarizability with density.

There exists a simple approximate formula to calculate the polarizability of a spherically symmetric atom:[43]

$$\alpha=\frac{4}{9a_0}\sum_i(\bar{r}_i^2)^2 \tag{22}$$

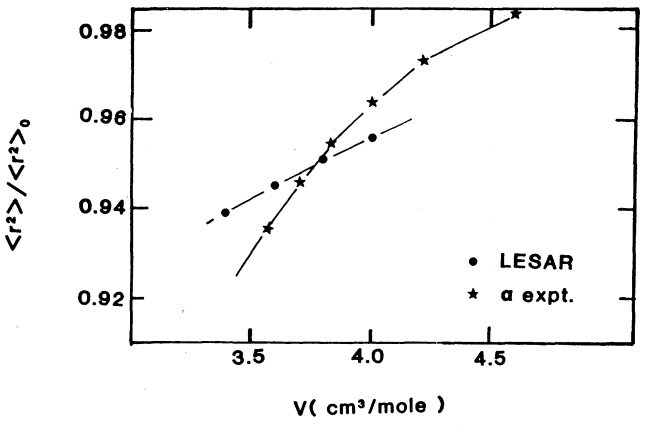

FIG. 9. Ratio of the mean-square radius of the crystal atomic wave function ($\langle r^2 \rangle$) to the gas value ($\langle r^2 \rangle_0$) as a function of volume for dense He. The dots are the calculations of LeSar (Ref. 29) and the stars the experimental determinations from Eq. (23).

which relates the polarizability to the extent of the electronic cloud, a_0 being the Bohr radius of the hydrogen atom, and r_i the position of electron i. Generally, a corrective multiplicative constant should be added in order to obtain a good agreement with experimental α. The observed decrease in $C(\rho)$ can consequently be directly related to the contraction of the electron cloud of an atom in the crystal which takes place in order to lower the repulsive interaction of an atom with its neighbors; as discussed above, this is the mechanism of the many-body interactions proposed by LeSar.[29] From Eq. (22) we can thus scale an experimental electronic cloud contraction:

$$\frac{\langle r^2 \rangle}{\langle r^2 \rangle_0} = \left[\frac{C(\rho)}{C(0)} \right]^{1/2} \tag{23}$$

and compare it in Fig. 9 to the one calculated by LeSar.[29] The agreement is quite good and it could even explain the discrepancy between LeSar EOS and the experimental one, as seen in Fig. 6. For volumes greater than 4 cm^3/mole, the theoretical contraction is less than the experimental one which means that the theoretical EOS should be below the experimental one (which is the case if we extrapolate LeSar EOS) but for volumes smaller than 3.7 cm^3/mol, it is the reverse and there his EOS is stiffer than the experimental one. The analysis of LeSar[29] clearly points out that there is a close relationship between the electronic properties of the system and the modeling of its interactions.

Finally, we believe that the analysis of the electronic properties of dense He in terms of the evolution of an excitonic level should be more appropriate to evaluate the predictions of the different *ab initio* calculations.

V. CONCLUSION

The present study reports accurate measurements of the refractive index of He up to 16 GPa that were made possible by the development of an original experimental interferometric method.

The determination of $n(P)$ is certainly important for diamond anvil cells high-pressure research since the refractive index is needed in the analysis of many optical measurements which are the main means of investigation of the properties of a sample under very higher pressure. As an example, the present $n(P)$ measurements on He were used in order to extract the adiabatic sound velocities from recently published[16] Brillouin frequency shifts.

These results then permit to go back to the thermodynamic properties of dense He, like the equation of state, the sound velocity, or the volume discontinuity at melting. Because fluid He extends over a very large density range, the present set of thermodynamic data could thus be quite useful for testing the validity of the theories of dense simple liquids, more specially $U(\rho)$ and $Cp/Cv(\rho)$ which are related to the second derivative of the free energy. Still, other single-crystal x-ray measurements would be welcome in order to reduce the error bars on the EOS; this is important for improving the description of the interactions in dense insulators which are still a subject of debate.

But the knowledge of $n(P)$ is essential if we want to probe the electronic properties of dense insulators in diamond anvil cells. The usual optical absorption measurements, related to the imaginary part of the dielectric constant, are inappropriate here since the absorption of the diamonds obscures everything. It is the first time that the evolution of the electronic properties of an insulator have been measured over such a large density domain. This is all the more interesting since He atom has only two electrons and so its system should be the most amenable to a theoretical attack. The present data could first be compared to recently proposed tight-binding calculations[1,29] and if necessary should stimulate the completion of new accurate methods of calculating the electronic band structure of insulators, which are known to be unsatisfactory up to now.[5]

Finally, the extension of the present measurements to higher density in He or to other more dispersive systems would require the determination of the dispersion of the refractive index; but this is of a higher degree of difficulty than the present study.

ACKNOWLEDGMENTS

We thank J. M. Besson and A. Polian for continuous interest in this work and many helpful discussions and J. L. Barrat for help in the quantum simulations of the EOS's of fluid He. We are grateful to M. Ross for communicating the results of his fluid variational calculation. We are thankful to the support of the Commissariat à l'Energie Atomique (France) under Grant No. C-1880-N2A and of the Groupement de Recherches Coordonnés de Structure Interne des Étoiles et des Planètes Géantes (Paris, France). The Laboratoire de Physique des Milieux Condensés is Unité Associée No. 782 du Centre National de la Recherche Scientifique.

[1]G. Senatore and K. R. Subbaswamy, Phys. Rev. B **34**, 5754 (1986).
[2]S. Raynor, J. Chem. Phys. **87**, 2790 (1987).
[3]B. J. Min, H. J. F. Jansen, and A. J. Freeman, Phys. Rev. B **33**, 6383 (1986).
[4]W. A. Harrison, Phys. Rev. B **31**, 2121 (1985).
[5]N. C. Bacalis, D. A. Papaconstantopoulos, and W. E. Pickett, Phys. Rev. B **38**, 6218 (1988).
[6]D. M. Ceperley, in *Simple Molecular Systems at Very High Density,* edited by A. Polian, P. Loubeyre, and N. Boccara (Plenum, New York, 1988), p. 477.
[7]D. M. Ceperley and B. J. Alder, Phys. Rev. B **36**, 2092 (1987).
[8]B. Sonntag, in *Rare Gas Solids,* edited by M. L. Klein and J. A. Venables (Academic, New York, 1976), p. 1021.
[9]K. Asaumi, T. Mori, and Y. Kondo, Phys. Rev. Lett. **49**, 837 (1982).
[10]J. van Straaten and I. F. Silvera, Phys. Rev. B **37**, 1989 (1988).
[11]M. Grimsditch, R. Le Toullec, A. Polian, and M. Gauthier, J. Appl. Phys. **60**, 3479 (1986).
[12]A. Jayaraman, Rev. Mod. Phys. **55**, 65 (1983).
[13]H. K. Mao, in Ref. 6, p. 221.
[14]R. Le Toullec, J. P. Pinceaux, and P. Loubeyre, High Press. Res. **1**, 77 (1988).
[15]M. Lallemand and D. Vidal, J. Chem. Phys. **66**, 4776 (1977).
[16]A. Polian and M. Grimsditch, Europhys. Lett. **2**, 849 (1986).
[17]R. D. McCarty, *Thermophysical properties of Helium-4 from 2 to 1500 K with pressures to 1000 atmospheres,* Nat. Bur. Stand. Technical (U.S.) Circ. No. 631 (U.S. GPO, Washington, D.C., 1972).
[18]P. J. Kortbeek, J. J. van de Ridder, S. N. Biswas, and J. A. Schouten, Int. J. Therm. **9**, 425 (1988).
[19]R. L. Mills, D. H. Liebenberg, and J. C. Bronson, Phys. Rev. B **21**, 5137 (1980).
[20]D. Vidal, L. Guengant, and M. Lallemand, Physica **96A**, 545 (1979).
[21]M. Ross (private communication).
[22]M. Ross, J. Chem. Phys. **71**, 1567 (1979).
[23]D. A. Young, A. K. McMahan, and M. Ross, Phys. Rev. B **24**, 5119 (1981).
[24]P. Loubeyre, D. Levesque, and J. J. Weis, Phys. Rev. B **33**, 318 (1986).
[25]R. A. Aziz, F. R. McCourt, and C. C. K. Wong, Mol. Phys. **61**, 1487 (1987).
[26]H. K. Mao, R. J. Hemley, Y. Wu, A. P. Jephcoat, L. W. Finger, C. S. Zha, and W. A. Bassett, Phys. Rev. Lett. **60**, 2649 (1988).
[27]J.-L. Barrat, P. Loubeyre, and M. L. Klein, J. Chem. Phys. **90**, 5644 (1989).
[28]P. Loubeyre, Phys. Rev. Lett. **58**, 1857 (1987).
[29]R. LeSar, Phys. Rev. Lett. **61**, 2121 (1988).
[30]F. Birch, J. Geophys. Res. **66**, 2199 (1961).
[31]P. Loubeyre and R. Le Toullec (unpublished).
[32]J. O. Hirshfelder, C. F. Curtiss, and R. Byron Bird, *Molecular Theory of Gases and Liquids,* (Wiley, New York, 1954), p. 232.
[33]P. Loubeyre, in Ref. 6, p. 181.
[34]L. van der Putten and J. A. Schouten, High Press. High Temp. **18**, 393 (1986).
[35]D. Frenkel, Phys. Rev. Lett. **56**, 858 (1986).
[36]B. J. Alder, H. L. Strauss, and J. J. Weis, J. Chem. Phys. **62**, 2328 (1975); B. J. Alder, J. C. Beers, H. L. Strauss, and J. J. Weis, Proc. Nat. Acad. Sci. U.S.A. **77**, 3098 (1980).
[37]R. F. Guertin and F. Stern, Phys. Rev. A **134**, 427 (1964).
[38]C. R. Mansfield and E. R. Peck, J. Opt. Soc. Am. **59**, 199 (1969).
[39]R. Peck, Appl. Opt. **22**, 2906 (1983).
[40]C. M. Surko, G. J. Dick, F. Reif, and W. C. Walker, Phys. Rev. Lett. **23**, 842 (1969).
[41]M. H. Edwards, Can. J. Phys. **36**, 884 (1958).
[42]A. C. Sinnock and B. L. Smith, Phys. Rev. **181**, 1297 (1969).
[43]J. O. Hirschfelder, C. F. Curtiss, and R. Byron Bird, Ref. 32, p. 946.